in cats," in *Summary Int. Microwave Power Symp.* (Ottawa, Ont., Canada, May 1972).
[4] A. W. Guy, J. C. Lin, and C.-K. Chou, "Electrophysiologic effects of electromagnetic fields on animals," in *Fundamental and Applied Aspects of Nonionizing Radiation*, 1974.
[5] E. M. Taylor, A. W. Guy, B. Ashleman, and J. C. Lin, "Microwave effects on central nervous system attributed to thermal factors," in *Dig. Tech. Papers, IEEE Int. Microwave Symp.* (Boulder, Colo., June 1973).
[6] C.-K. Chou and A. W. Guy, "Effect of 2450 MHz microwave on peripheral nerve," in *Dig. Tech. Papers, IEEE Int. Microwave Symp.* (Boulder, Colo., June 1973).
[7] R. M. Eccles, "Action potentials of isolated mammalian sympathetic ganglia," *J. Physiol.*, vol. 117, pp. 181–195, 1952.
[8] B. Libet, "Generation of slow inhibitory and excitatory postsynaptic potentials," *Fed. Proc.* (Abstr.), vol. 29, pp. 1945–1956, 1970.
[9] S. D. Erulkar and J. K. Woodward, "Intracellular recording from mammalian superior cervical ganglion in situ," *J. Physiol.* (London), vol. 199, pp. 189–203, 1968.
[10] U. Trendelenburg, "Some aspects of pharmacology of autonomic ganglion cells," *Ergeb. Physiol.*, vol. 9, pp. 1–85, 1967.
[11] I. Yamaura and S. Chichibu, "Superhigh frequency electric field and crustacean ganglionic discharges," *Tohoku J. Exp. Med.*, vol. 93, pp. 249–259, 1967.
[12] H. Wachtel, R. Seaman, and W. Joines, "The effects of microwaves on isolated neurons," presented at the *N. Y. Acad. Sci. Conf. Biological Effects Non-ionizing Radiation*, Feb. 1974.

Nonreciprocal Delay Line for Use in S Band Tubes

ROBERT J. TIERNAN AND ERNST SCHLÖMANN, SENIOR MEMBER, IEEE

***Abstract*—In an effort to make ferrites available for broad-band resonance isolator applications in high-power mirowave tubes, seven lithium ferrites and four nonlithium spinel ferrites were tested for resonance-loss behavior near an S band (2.0–4.0-GHz) linear helix.**

The observed behavior, i.e., the dependence of the absorption on the dimensions of the ferrites, can be attributed to excitation of surface magnetostatic modes. Using the results of the Damon–Eshbach theory for surface magnetostatic modes in semi-infinite slabs, resonance frequency and surface-wave attenuation factors were numerically calculated as a function of the propagation coefficient and the ratio of magnetization to internal field.

I. INTRODUCTION

THE ability of ferrites, biased by magnetic fields, to act as isolators and phase shifters, has been known for a long time, and in many cases ferrites have been used external to high-power microwave tubes to protect them from load mismatch. For many years there has been a need for ferrites inside high-power tubes to improve their efficiency and, in the case of pulsed operation, decrease the turn-on time. In crossed-field amplifier (CFA) tubes, ferrites were needed as unidirectional attenuators in band. Ferrites were not used in tubes previously because spinel ferrites tended to give off gases when heated up, and to become dielectrically lossy when assembled inside tubes, whereas garnet ferrites never offered the range of saturation magnetization or Curie temperature to make them suitable. Improvements in spinel-ferrite fabrication through the years and recent work at Raytheon [1] has shown, however, that in regard to spinel ferrites, the previously experienced difficulties can be overcome.

The major difference between designing ordinary isolators and isolators for use inside tubes is the fact that for tubes the magnetic field strength is generally fixed by other requirements. This means that the resonance frequency of the isolator must be adjusted to the desired value by suitable choice of other parameters such as the sample shape, the saturation magnetization, and the effective gyromagnetic ratio g_{eff}. Additional constraints upon the isolator design are imposed by the requirement that it should work with the existing tube structure without the need for any modification. It is, therefore, very important to be able to predict the performance of a tube isolator with some accuracy, because a purely empirical design procedure would be very costly.

There are several equations for predicting the frequency at which a specific ferrite will exhibit resonance loss: the equation selected depending on boundary conditions, ferrite geometry, propagation constant, and the like. Each equation requires that one know the saturation magnetization $4\pi M$, the internal magnetic field strength, and the effective gyromagnetic ratio g_{eff} of the polycrystalline ferrite. The theories from which the equations originate are based on assumptions regarding the wavelength of the RF signal relative to ferrite dimensions, the polarization of the RF field relative to the magnetic field and propagation direction, the uniformity of the biasing and RF field throughout the ferrite region, and the degree of saturation of the ferrite. Seldom are all requirements for a given theory satisfied in practice. Vendors in general state the X band g_{eff} in catalog listings. The g_{eff} [2] for ferrite spheres are, in general, frequency dependent due to the

Manuscript received January 9, 1975; revised May 7, 1975.
R. J. Tiernan was with the Raytheon Microwave Tube Operation, Waltham, Mass. 02154. He is now with the Argonne National Laboratory, Argonne, Ill. 60439.
E. Schlömann is with the Raytheon Research Division, Waltham, Mass. 02154.

presence of finite porosity, anisotropy, and magnetostrictive fields, and can deviate significantly from the single-crystal g-value (which is approximately 2), particularly at low frequencies. Preliminary measurements at Raytheon on some spinel-ferrite slabs of nonzero porosity at S band frequencies have verified this. Internal fields are in general a function of position in ferrites of practical geometries. In order to properly select an internal field for use in the equations, one must know over what region of the ferrite the RF wave that is to be attenuated is interacting with the precessing magnetic moments. This paper will present an equation for routinely predicting frequencies of ferrite resonance loss from 2.0 to 4.0 GHz when they are mounted near a helix-type delay line. Theoretical predictions will be compared with measured values, the latter being made possible through specific measurements to determine internal fields, and through numerical calculations of demagnetizing factors for ferrites of finite size.

II. TEST PROCEDURE

Fig. 1 shows the inside of a typical S band CFA tube. The RF wave propagates in a helical path around the tube periphery with a reduced velocity $\approx c/12$, where c is the velocity of light in vacuum, and interacts with an electron stream coming from the cathode (not shown) which is concentric with the slow-wave structure. An axial magnetic field is applied to the tube to induce an azimuthal velocity to the electrons resulting in interaction of the electron stream with the RF field, and amplification. To use ferrites as unidirectional attenuators they are mounted under the helix on the back wall—the insert in Fig. 1 shows this for one piece of ferrite and one turn of the helix—where the RF magnetic field has a circularly polarized component. The dc field magnitude at this position was measured to be 1240 Oe. In order to perform the many tests on the ferrites used in this work, a linear helix, which was identical in structure to the circular one, was used. An electromagnet with 9 × 9-in pole pieces created uniform fields over the plane of the ferrite and along the entire helix length. Fields were measured with a Hall probe and conventional null meter. The initial objective of this project was to improve the performance of S band CFA tubes, such as in Fig. 1 by the use of spinel ferrites. The dimensions of the ferrites were therefore varied to locate loss peaks in this band at fields of 1240 Oe. The best unidirectional loss pattern was obtained with cross-sectional dimensions of 0.210 × 0.105 in. The analysis in this work was therefore based on ferrite slabs of these dimensions. Insertion-loss measurements were carried out from 2.0 to 4.0 GHz with a Hewlett-Packard network analyzer. An S parameter test set was used to conveniently switch direction of the RF signal, thereby simulating a forward and reverse propagation.

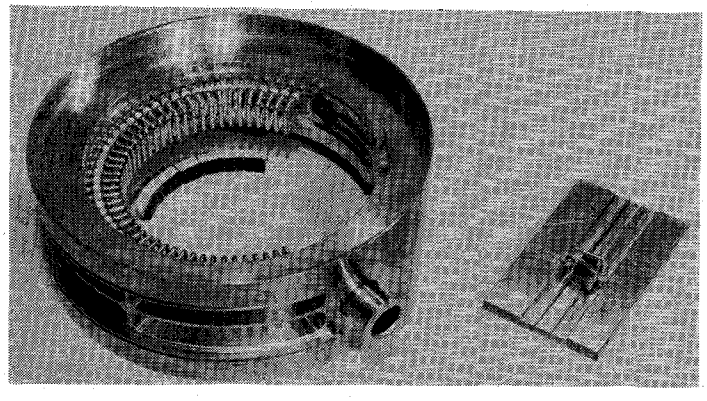

Fig. 1. S band CFA tube with nonreciprocal delay line.

The general procedure was to observe on a scope the insertion loss over the 2.0–4.0-GHz band, while the magnetic field was increased from zero. When the gyromagnetic resonance-loss peak occurred in band, a trace was made of the pattern using a Mosely recorder. A reference trace was made by increasing the magnetic field well above the value for any gyromagnetic resonance loss in band, fully saturating the ferrite. This latter trace corresponded to the insertion loss of the helix–ferrite combination, where the ferrite was acting strictly as a high permittivity dielectric.

Reflection measurements were made using the same equipment in order to verify that the observed loss in the ferrites was due to absorption. Reflection loss was 8–11 dB below absorption loss in all cases.

The g_{eff} were measured at 3.05 GHz using an S band spectrometer and annealed ferrites that were in the shape of spheres 2.25 mm in diameter. A TE-103 transmission cavity was used. The biasing field was varied until transmission resonance was observed. The field was then measured with a Hall probe and g_{eff} obtained from the equation [2]

$$f = \frac{e}{4\pi mc} g_{\text{eff}} H_0 \tag{1}$$

where e and m are the electric charge and the mass of the electron, respectively, c is the velocity of light in vacuum, and H_0 the magnetic field strength. To a good approximation $e/4\pi mc = 1.4$ MHz/Oe.

III. COMPARISON OF EXPERIMENT WITH THEORY

Figs. 2 and 3 show typical insertion-loss data for a lithium ferrite and a nonlithium ferrite, respectively. The curves, designated as $+I_0$ and $-I_0$ were the forward and reverse propagating signal, respectively, the third curve being the "reference" trace. Resonance-loss peaks also occurred for the "forward" propagating wave in these and all other ferrites (seven lithium ferrites and four nonlithium spinel ferrites) at frequencies about 8–10 percent higher than the reverse peak. Their origin has not been investigated in detail. All reverse loss peaks were significantly asymmetric.

The S band g_{eff} for the nonlithium ferrites were 2.00 to within a few percent. For the lithium ferrites, the g_{eff} differed significantly from 2.00 as indicated by Table I.

If the Kittel equation for uniform mode precession

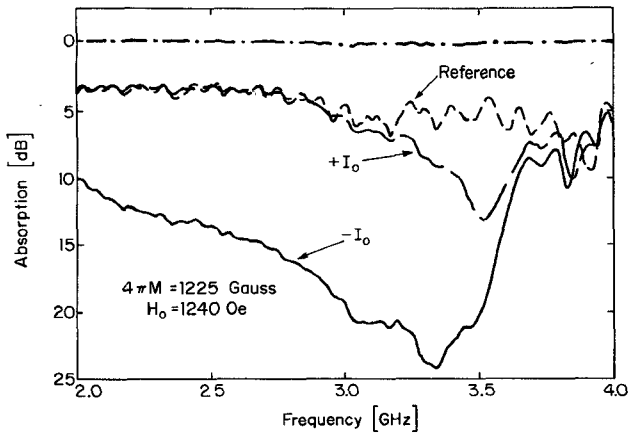

Fig. 2. Frequency dependence of the insertion loss for a lithium ferrite. The curves labelled $+I_0$ and $-I_0$ correspond to the two directions of propagation. The reference curve is measured at a very high magnetic field strength, where the ferrite behaves substantially as a dielectric.

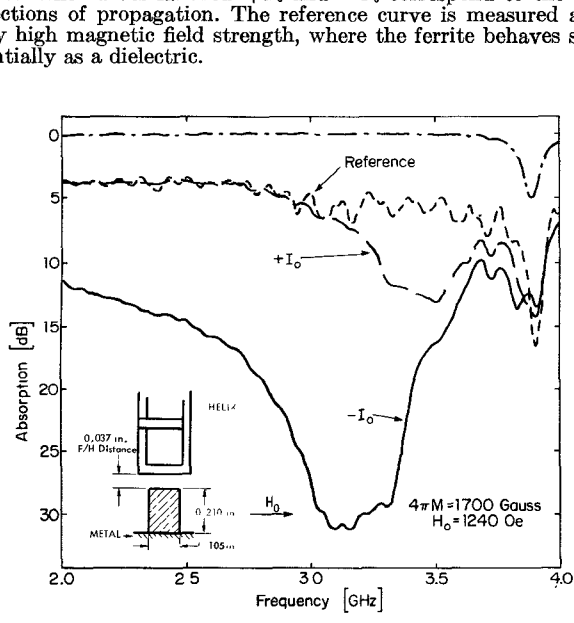

Fig. 3. Frequency dependence of the insertion loss for a nonlithium spinel ferrite. The inset shows the ferrite–helix configuration used in all of the experiments reported in the paper. The curves have the same significance as in Fig. 2.

TABLE I
FREQUENCY OF REVERSE LOSS PEAKS OF LITHIUM FERRITES

$4\pi M_0$(Gauss)	Curie Temp. (°C)	g_{eff}	$f_{meas.}$ (GHz)	f_A(GHz)	f_{Kittel}(GHz)
810	330	2.20	3.05	2.82	2.03
1040	372	2.33	3.00	2.74	1.72
1225	312	2.18	3.05	2.84	1.63
1270	320	2.22	2.90	2.80	1.53
1404	350	2.90	2.87	2.73	1.05
1770	445	2.08	2.95	2.78	0.53
2050	490	3.62	3.74	3.34	1.11

Note: f_A is based on (9) and $N_z(0,0)$.

$$f = \frac{e}{4\pi mc} g[H_0 - (N_z - N_x)4\pi M]^{1/2} \cdot [H_0 - (N_z - N_y)4\pi M]^{1/2} \quad (2)$$

were used to predict the resonance frequencies using the average bulk value for the demagnetizing factor, frequencies about one-half of the observed ones would result.

It should not be surprising that the Kittel equation does not agree with the observed frequencies in this case because the RF field in the ferrites near delay lines is nonuniform (decaying exponentially away from the helix), and the wavelength of the guided wave (~0.83 cm) is not large compared to the dimension of the ferrite (0.53 × 0.25 × 15.24 cm). Qualitatively, therefore, the observed loss behavior is arising from the interaction of a slow EM wave, guided by the helix, with a magnetostatic surface wave guided by the ferrite–air interface. A dispersion relation for these modes has been worked out [3], [4] based on a semi-infinite sheet of thickness $2a$ in the x direction. z and y are the magnetic field and propagation directions, respectively. For this case the dispersion relation can be expressed as

$$2\mu\bar{k}_x\alpha \coth (2\bar{k}_x a) = -\mu^2\bar{k}_x^2 + \kappa^2 k_y^2 - \alpha^2 \quad (3a)$$

$$\mu(-\bar{k}_x^2 + k_y^2) + k_z^2 = 0 \quad (3b)$$

$$\alpha = (k_y^2 + k_z^2)^{1/2} \quad (3c)$$

where k_y and k_z are the wavenumber components for the y and z directions. The wave decays exponentially in the x direction with the decay constant $\bar{k}_x$, and μ and κ are the diagonal and off-diagonal components of the permeability tensor

$$\mu = \frac{BH_i - (\omega/\gamma)^2}{H_i^2 - (\omega/\gamma)^2}, \qquad \kappa = \frac{4\pi M(\omega/\gamma)}{H_i^2 - (\omega/\gamma)^2},$$

$$B = H_i + 4\pi M. \quad (4)$$

The following reduced notation has been used in the evaluation of the dispersion relation (3):

$$2\bar{k}_x a = x, \qquad 2k_y a = y, \qquad 2k_z a = z,$$

$$m = \frac{4\pi M}{H_i}, \qquad \Omega = \frac{\omega}{\gamma H_i}. \quad (5)$$

From (3) and (4) the reduced frequency Ω can be expressed in terms of the reduced wavenumbers y and z

$$\Omega^2 = 1 + m + m\frac{z^2}{x^2 - y^2 - z^2} \quad (6)$$

where x is to be determined from

$$2z^2(y^2 + z^2)^{1/2} x \coth x = (my^2 - z^2)x^2 - (y^2 + z^2)(my^2 + z^2). \quad (7)$$

Equation (7) has been solved numerically for x (with given y, z, m). The solid lines in Fig. 4 show Ω versus y for $m = 6$ and z^2 from 0 to 40. Fig. 5 is a plot of Ω versus y and x versus y for $m = 10$ and $z^2 = 1.0$.

The numerical solution of (7) upon which these results are based is a rather involved calculation. For many cases of interest $x \gg 1$, so that the coth in (7) can be replaced by unity. In this limit (7) becomes a quadratic equation for x. Substituting the solution into (6) yields

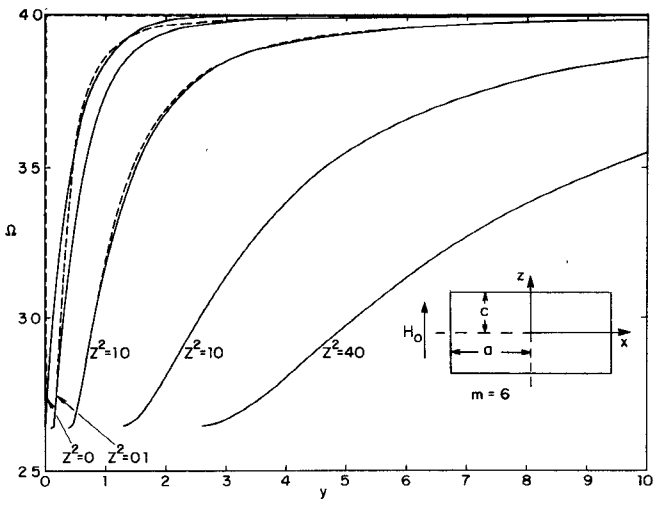

Fig. 4. Calculated dependence of the frequency Ω of magnetostatic surface waves upon the wavenumber y on reduced scales. The broken lines are the result of an approximate theory described in the text.

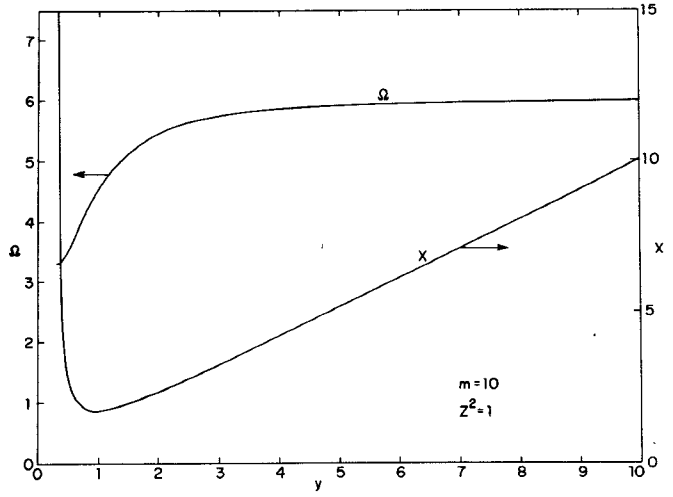

Fig. 5. Calculated dependence of the frequency Ω and of the transverse decay constant x upon the wavenumber y on reduced scales.

$$\Omega^2 = 1 + m + \frac{(my^2 - z^2)^2}{4y^2(y^2 + z^2)}. \tag{8}$$

Dispersion diagrams derived from this equation are indicated by broken lines in Fig. 4. The broken lines are not shown separately where they coincide with solid lines. For the application of (8) it must be kept in mind that (7) has real solutions x only when $my^2 - z^2 > 0$.

For the limiting case of $z \to 0$, (6) becomes [since $x \to y$ and $(x^2 - y^2)/z^2 \to 2m^{-1}(\coth y + 1) + 1$]

$$\Omega^2 = 1 + m + \frac{m^2}{4}[1 - \exp(-2y)]. \tag{9}$$

Maximum interaction between the magnetostatic wave and the helix-guided wave is expected to occur when the propagation constants k_y are equal. Under typical experimental conditions $y \simeq 4$ ($3.3 \leq y \leq 5.3$ for 2.5 GHz $\leq f \leq$ 4.0 GHz). Thus the exponential in (9) can be neglected to a good approximation, so that

$$\Omega = 1 + \tfrac{1}{2}m. \tag{10}$$

The attenuation factor x is equal to y for the case $z = 0$, which implies that the intensity of the surface magnetostatic modes falls off to $1/e$ of its value at the surface in 0.133 cm (0.053 in).

The preceding analysis applies, strictly speaking, to a semi-infinite slab (i.e., z and y dimensions much greater than $2a$). If the slab is finite in both the x and z directions, it appears likely that the same analysis can be used by way of an approximation. In this case, however, a possibility of a nonzero k_z exists. One may expect that the width of the sample $2c$ corresponds to half a wavelength. This implies that

$$k_z = \frac{2\pi}{4c} = \frac{\pi}{2c}, \qquad z = 2k_z a = \pi\frac{a}{c} \tag{11}$$

i.e., $z = 6.28$ for the case of all ferrite slabs tested in this work. Magnetostatic surface waves with $k_z \neq 0$ exist only when $m > k_y^2/k_z^2$ [see (7)], i.e., in the present case ($y \simeq 4$, $z = 6.28$) when $m > 2.5$.

In order that (9) or (11) be used to predict resonance frequencies, the internal field H_i has to be known for the finite size rectangular cylinders used in this work. Consequently, the demagnetizing factors were determined in an approximate fashion, based on the assumption that the sample is uniformly magnetized, and magnetized to saturation [5]. The local demagnetization factor of first order is, for a long slab of cross-section dimension $2a \times 2c$,

$$\begin{aligned} N_z(x,z) = N_{zz}^{(1)}(x,z) = (1/2\pi)[&\cot^{-1} f(x,z) \\ &+ \cot^{-1} f(-x,z) + \cot^{-1} f(x,-z) \\ &+ \cot^{-1} f(-x,-z)] \end{aligned} \tag{12}$$

where

$$f(x,z) = \frac{c - z}{a - x}. \tag{13}$$

Thus at the center of the cylinder cross section

$$N_z(0,0) = (2/\pi)\cot^{-1}(c/a) \tag{14}$$

and at the center of the sideface

$$N_z(a,0) = (1/\pi)\cot^{-1}(c/2a). \tag{15}$$

Since the surface wave extends over all of the sideface of the cylinder, one should probably use an average of N extended over this sideface. This average is, according to (12) and (13),

$$\begin{aligned} \langle N_z(a,z)\rangle = (1/c)\int_0^c dz\, N_z(a,z) = (1/\pi)[&\cot^{-1}(c/a) \\ &+ (a/2c)\ln\{1 + (c/a)^2\}]. \end{aligned} \tag{16}$$

A graph of $N_z(0,0)$, $N_z(a,0)$, and $\langle N_z(a,z)\rangle$ as functions of c/a is given in Fig. 6. For $c/a < 1$ (for our case $c/a = 0.5$)

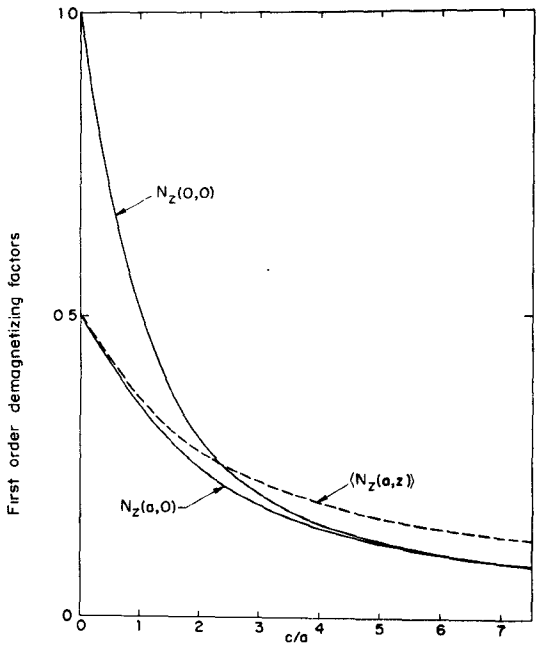

Fig. 6. Calculated demagnetizing factors for a long rectangular slab. $N_z(0,0)$ applies to the center of the slab, $N_z(a,0)$ to the center of a sideface, and $\langle N_z(a,z)\rangle$ represents the average over a sideface.

the difference between $N_z(a,0)$ and $\langle N_z(a,z)\rangle$ is quite small.

The H_i occurring in (4) and (5) are the internal fields in the regions of the ferrite where the RF field is interacting with the magnetostatic modes

$$H_i = H_0 - 4\pi M\langle N_z(x_0,z)\rangle + \hat{H} \qquad (17)$$

where H_0 is the applied field, $\langle N_z(x_0,z)\rangle$ is the demagnetizing factor, averaged over z, at some mean value x_0 in the ferrite slab, $\hat{H}$ is a "built-in" magnetic field arising from anisotropy and porosity (we are neglecting magnetostrictive effects). $\hat{H}$ is obtained from the "effective g" derived from (1) and the following equation [2]

$$\hat{H} = (f4\pi mc/e)[1/g - 1/g_{\text{eff}}] \qquad (18)$$

where f is the frequency in megahertz, and g is the spectroscopic splitting factor applicable to a single crystal of the same composition. By way of approximation we take $g = 2$. As a first approximation, $\langle N_z(x_0,z)\rangle$ was taken as $N_z(0,0)$ for the case $k_z = 0$ [see (10)] and as $N(a,0)$ for the case $k_z \neq 0$ [see (11)] since the attenuation of the magnetostatic waves is much larger in the latter case. Referring to Fig. 6 (and noting that $c/a = 0.5$ for all ferrites tested), the values for N_z are 0.725 and 0.425, respectively.

Table II lists the H_i and m for all ferrites tested near the delay line. H_i and m have been calculated according to (17) and (5) taking for $\langle N_z(x_0,z)\rangle$ the two values applicable for the bulk ($N_z = 0.725$, subscript A) and the surface ($N_z = 0.425$, subscript B) of the sample. It may be seen that m_B is smaller than the critical value 2.5 derived in connection with (11) for all except two of the samples tested. Thus the observed loss peaks cannot be

TABLE II
MAGNETIC PARAMETERS OF FERRITES USED IN EXPERIMENTS

Type	$4\pi M$ [Gauss]	H_{iA} [Oe]	m_A	H_{iB} [Oe]	m_B
Lithium Ferrite	810	543	1.50	786	1.03
	1040	390	2.67	703	1.48
	1225	324	3.78	693	1.77
	1270	283	4.45	663	1.92
	1404	180	7.85	603	2.34
	1770	≈ 0	----	526	3.37
Non-Lithium Spinel Ferrite	750	695	1.08	922	0.81
	1000	515	1.94	815	1.23
	1300	296	4.40	686	1.90
	1750	≈ 0	----	496	3.53

Note: H_{iA} and m_A are based on using $N_z(0,0)$ for $\langle N_z(x_0,z)\rangle$ in (17). H_{iB} and m_B are based on using $N_z(a,0)$.

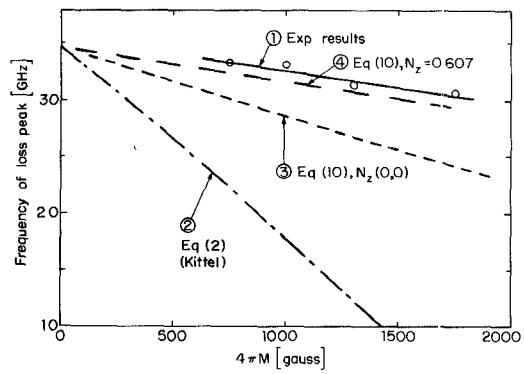

Fig. 7. Experimental and theoretical dependence of the loss-peak frequency upon the saturation magnetization of the ferrite.

attributed to magnetostatic surface waves with $k_z \neq 0$ and given by (11).

Fig. 7 is a plot of f (in gigahertz) versus $4\pi M$ (in gauss) for the nonlithium ferrites based on experimental results and the predictions of the various equations. Curve 1 represents the experimental data. Curve 2 is based on (2), the Kittel resonance condition. Curve 3 is based on (10) taking the bulk demagnetizing factor. Using (10) with the surface demagnetization factor $N_z(a,0)$ produced a curve higher in frequency than the measured frequencies with a positive slope, hence it was not plotted. Curve 3, which agrees with the observed frequencies to within 10 percent for low-$4\pi M$ materials, and to within 20 percent for high-$4\pi M$ materials, corresponds to a "$k_z = 0$" surface mode. Taking $N_z(0,0)$ as the effective demagnetizing factor assumes that there is significant penetration of the surface modes throughout the ferrite in the $\hat{x}$ direction. The curve using Kittel's equations (curve 2) is a factor of at least 2 below the experimental curve.

Equation (10) can be expressed in terms of H_0 and $4\pi M$ as

$$f = \frac{e}{4\pi mc} g[H_0 - \{\langle N_z(x_0,z)\rangle - 1/2\}4\pi M]. \qquad (19)$$

This is curve 3 in Fig. 7 with $\langle N_z(x_0,z)\rangle$ taken as $N_z(0,0)$.

However, if a straight line is fitted to the experimental points in Fig. 7 (curve 1) using a least square fitting procedure the intercept at $4\pi M = 0$ yields an H_0 of 1265 Oe, in good agreement with the external field of 1240 Oe used for these ferrites. The slope yields an $\langle N_z(x_0,z)\rangle$ of 0.607 which lies between the value of $N_z(a,0)$ and $N_z(0,0)$ (see Fig. 6). If this latter value is used for $\langle N_z(x_0,z)\rangle$ in (19), the agreement with the experimental curve is improved as shown by curve 4 in Fig. 7. This curve now predicts frequencies within three percent of the observed ones.

For the lithium ferrites, curves of the type displayed in Fig. 7 could not be set up because g_{eff} was not constant from sample to sample. Table I compares the measured frequencies of the reverse loss peaks of these lithium ferrites with those predicted from (10). The agreement is better than 8 percent; however, it is important to note that separate g_{eff} measurements had to be made at S band in order to arrive at accurate values of H_i.

Insertion-loss measurements have also been made on ferrite slabs of various thicknesses in the x direction (0.020 in $\leq 2a \leq$ 0.060 in), the ferrite-to-helix distance being held constant. The measurements showed that the insertion loss increases moderately with the ferrite thickness. This is in qualitative agreement with our interpretation of the resonant frequencies in that it confirms that the excitation is not tightly confined to the sample surface.

IV. CONCLUSION

Two simple equations [(8) and (10)] have been derived and compared with the observed resonance-loss frequencies of ferrites near S band delay lines. The comparison has shown that (10), which corresponds to $k_z = 0$, agrees with the measured frequencies to within 3 percent, if a value of N_z somewhere between surface and bulk (but closer to bulk) values is chosen.

If the effective g-value of the polycrystalline material differs substantially from the single-crystal value ($\simeq$2), as was the case for the lithium ferrites used in the present experiments, a separate determination of g_{eff} in the frequency band of interest is necessary in order to derive reliable estimates of the frequency at which the delay line has maximum absorption.

REFERENCES

[1] R. J. Tiernan, L. H. Tisdale, and S. B. Besse, "Technology of incorporation of internal ferrites in microwave power tubes," *Amer. Ceram. Soc. Bull.*, to be published.
[2] P. J. B. Clarricoats, *Microwave Ferrites*. New York: Wiley, 1961, pp. 56 and 57.
[3] R. W. Damon and J. R. Eshbach, "Magnetostatic modes of a ferromagnetic slab," *J. Phys. Chem. Solids*, vol. 19, pp. 308–320, 1961.
[4] E. Schlömann and R. I. Joseph, "Spin waves and magnetostatic waves," Raytheon Tech. Rep. R-68, Mar. 1968, pp. 30–39, unpublished.
[5] R. I. Joseph and E. Schlömann, "Demagnetizing field in nonellipsoidal bodies," *J. Appl. Phys.*, vol. 36, pp. 1576–1593, May 1965.

An Annotated Bibliography of Microwave Circulators and Isolators: 1968-1975

REINHARD H. KNERR, SENIOR MEMBER, IEEE

Abstract—**A bibliography of microwave circulators and isolators from 1968 to 1975 is presented. Some observations on selected topics are made.**

INTRODUCTION

THIS PAPER presents a bibliography building on the one published in an earlier review paper.[1] As such, it precludes the reexamination of most of the more fundamental papers which were published before 1968. The literature is not critically surveyed; rather, some observations on selected topics are made. The emphasis on different contributions is somewhat influenced by the author's own background and experience.

In the years after 1968, microwave circulator and isolator[2] design techniques have matured and have been furthered by systematic, scientific studies. Waveguide circulators have become better understood and the computer has been successfully applied to solve the awkward boundary value problems for some of the simpler structures. In the next section, the renewed effort to use S-parameter eigenvalues for circulator design will be reviewed in more detail.

Manuscript received August 23, 1974; revised April 18, 1975.
The author is with Bell Laboratories, Allentown, Pa. 18103.
[1] R. F. Soohoo, "Microwave ferrite materials and devices," *IEEE Trans. Magn.*, vol. MAG-4, pp. 118–133, June 1968.

[2] Since circulators are frequently used as isolators by terminating one port, all comments concerning circulators apply to those as well.